Determination of the unsaturated hydraulic conductivity of clayey samples using magnetic resonance imaging (MRI)

Sandrine Rosin-Paumier, Sébastien Leclerc, Adel Abdallah, Didier Stemmelen

Determination of the unsaturated hydraulic conductivity of clayey samples using magnetic resonance imaging (MRI).

Rosin-Paumier, S., Leclerc, S., Abdallah, A. & Stemmelen, D.
LEMTA (CNRS, UMR 7563) 2 avenue de la Forêt de Haye, BP 160, F-54504, Vandoeuvre-lès-Nancy Cedex, France

ABSTRACT: In some conditions, soils are submitted at the same time to thermal and hydraulic solicitations. Under these variations, the unsaturated hydraulic conductivity (k_u) of the soil evolves. The determination of the time evolution of the water content profile inside the samples is necessary to calculate k_u but its establishing is complex. In this study, a Magnetic Resonance Imaging method named Single Point Imaging was used. First, a calibration curve connects the MRI signal to the water content of samples prepared at various water contents and densities. Then the method is applied on clayey sample (argillite) submitted to two drying tests of at least 4 days at 20 or 40°C. The imposed hygrometry was 33%. Finally, the Instantaneous Profile Method was used to determine k_u values from water content profiles. This method was successful in recording the impact of the heating on the drying kinetics.

1 INTRODUCTION

In several environmental applications, soils are submitted at the same time to thermal and hydraulic solicitations. Variations may be natural, such as weather conditions or anthropogenic, such as heating linked to waste storage or geothermal probe. Under these variations, the hydraulic properties, including the unsaturated hydraulic conductivity (k_u) of the soil, evolves. This parameter is especially important in the context of the nuclear waste repository. Indeed, Tsang et al. (2011) explain that between completion of excavation and lining installation and the emplacement of waste and buffer, the rock wall is in contact with the atmosphere. In particular, tunnel ventilation can desaturates the rock wall and modifies its hydraulic properties. The determination of k_u requires the knowledge of the water content profile inside the rock, a very complex task. Classical methods may perturb the integrity of the sample, a fact which prevents to follow the time evolution of the hydraulic parameters.

Nuclear Magnetic Resonance (NMR) spectroscopy is a powerful tool for the determination of complex structures and their interactions. It can be used on materials containing several phases. An application of this technique, Magnetic Resonance Imaging (MRI), can be used to locate the NMR signal inside the sample. First MRI experiments were performed on living tissues for medical applications. Then, new methods were developed to obtain images of objects such as soil samples (Amin et al. 1996). Simpson et al. (2011) reviewed the evolution of MRI techniques in soil sciences from the establishing of calibration curves between the NMR signal and the water content of the sample (Prebble & Currie 1970) to the acquisition of three dimensional maps of structured soils. For example, Amin et al. (1996) used a spin-echo pulse sequence to study the water infiltration in a heterogeneous soil. This method provides a visual and non-destructive means to monitor the temporal changes of soil water content, and movement of the wetting front. It allows identifying preferential flow pathways in the soil. Magat (2008) studied the microstructural evolution of cementitious materials during hydration process and analyzed modifications due to drying effect. Dvinskikh et al. (2009) obtained images of both material and water content distribution in a sample and demonstrated their use for studying the swelling of bentonite clay with water.

However, it was difficult to apply these processes to soils, especially clayey soils, because they contain metallic elements. Indeed, these metal elements decrease the NMR relaxation times, which prevent classical methods to be used. Moreover, the interpre-

tation of the signal depends on the water interactions with the soil particles. On the one hand, the relaxation time of free water is long enough to use the classical spin-echo protocols. On the other hand, the numerous interactions between the water and the clayey layers decrease the relaxation time (< 5ms) and prevent the use of classical method. Specific methods were developed to solve these problems.

In this study, a MRI method named Single Point Imaging (SPI), developed by Emid & Creyghton (1985) was applied on several clayey samples. In the SPI technique, a single point of the free induction decay is detected a short time after the excitation pulse (Koptyug 2012). In this technique, the encoding time is very short and the magnetic gradients are strong. As a result, the method solves the short relaxation time problem. However, this method has to be applied on a single point and must be repeated for each point after the return to equilibrium. The run may be lengthy but allows the location of water in the porous matrix. Measurements can be 1D, 2D and 3D. The method was applied on argillite powder, compacted at various water contents and densities in order to acquire a calibration curve which connects MRI signal to water content of samples. The method was then applied to a raw argillite sample subjected to various controlled thermal and hydraulic solicitations. The evolution of the water content inside the sample was observed over time. These results allow calculating k_u according to the following method.

Several laboratory testing techniques are available to determine hydraulic properties such as k_u (Masrouri et al. 2008). The Instantaneous Profile Method (IPM) consists of inducing transient flow in a long cylindrical sample of soil and then measuring the resultant water content and/or pore water pressure profiles at various time intervals (Hamilton et al. 1981). k_u is then computed by using transient profiles of water content and pore water pressure head in conjunction with Darcy's law. To measure the pore water pressure profile, Wind (1968) proposed a direct evaporation technique in laboratory. It provides an estimation of the water retention and the hydraulic conductivity curves. In this study, the water content in each point of the sample was measured using the MRI technique and the pore water pressure was calculated thanks to a pre-established water retention curve. Then, the IPM allows converting w profiles in k_u values.

In this study, the used material (COX argillite) and methods (SPI, IPM) are presented in the first part as well as details on the sample preparation. The second part consists of the results and discussions before to conclude.

2 TESTED MATERIAL AND METHODS

In this part we first introduce the MRI method. In a second part, the instantaneous profile method is explained. Third, the COX argillite, used in this study is characterized. Finally, the sample preparation procedure is detailed.

2.1 *MRI method*

The measurements were performed using MRI equipment operating at 100 MHz (Bruker Biospec 24/40). A Single Point Imaging sequence was used to obtain the signal intensity. The experimental parameters were chosen as follows: angle $\alpha = 4.5°$ (5 µs), 64 measurement points, magnetic field B_0 = 2.34 T, MRI probe: 35 mm in diameter (Rapid Biomedical GmbH), maximal gradient: 200 mT/m, evolution time 40 µs < τ < 180 µs.

In an image acquired with the SPI method (Young et al. 2006), the intensity of each voxel (S) is:

$$S = M_0 \exp\left(\frac{-\tau}{T_2^*}\right) \quad (1)$$

Where: S = intensity of a voxel; M_0 = magnetization in a pixel; τ = encoding time; T_2* = transverse relaxation time.

M_0 is related to the water quantity in the considered voxel. In order to measure this value, τ has to be reduced as low as possible so that the impact of the relaxation time is minimized. However, as the resolution is a function of τ times the magnetic field gradient, and as this last parameter is limited by the hardware, one can achieve very low encoding times only by decreasing spatial resolution. Moreover, as the relaxation time evolves with the water content, S is not entirely proportional to water content. Consequently, to obtain a quantitative map of water content in a clay, a calibration curve connecting T_2* and w has to be achieved. In order to do so, several images are acquired at various τ and the regression of the experimental points with Equation 1 allows to determine T_2*. The method was applied to samples of known w in order to determine the calibration curve before being used on raw samples submitted to drying tests.

2.2 *The instantaneous profile method*

The retention curve of the material is necessary to calculate the matrix suction of the material. Suction (s) is calculated using the van Genuchten equation (van Genuchten 1980):

$$\Psi = \frac{1}{\alpha}\left[\frac{1}{(S_e)^{\frac{1}{m}}} - 1\right]^{\frac{1}{n}} \quad (2)$$

Where Ψ = negative pore water pressure or suction (MPa); S_e = effective water saturation; α (MPa^{-1}), m and n = van Genuchten parameters obtained by fitting the model to experimental data.

At each depth, the flow velocity and the hydraulic gradient are calculated from water content profiles and suction profiles respectively. Then, the unsaturated hydraulic conductivity is determined using Darcy law:

$$k_u = \frac{v}{\frac{d\Psi}{dz} \pm 1} \quad (3)$$

Where k_u = unsaturated hydraulic conductivity ($m.s^{-1}$); v = flow velocity ($m.s^{-1}$); $d\Psi/dz$ = hydraulic gradient.

2.3 *COX Argilite*

The studied argillite comes from the callovo-oxfordian level (COX) from the Parisian basin. Huang (2012) described this argillite formation as a heterogeneous medium in which the quartz and large calcite grains are dispersed in a fine matrix of clay minerals and calcite, which acts as cement for the larger grains. The mineralogy, obtained by Abou-Chakra Guéry et al. (2008), showed a composition of quartz (23% average), calcite (28% average), and clay minerals (45% average) together with subordinate feldspars, pyrite, and iron oxides (5% average). The clay mineral composition is relatively constant at 65% I/S (illite–smectite interstratified minerals), 30–35% illite, and 0–5% kaolinite and chlorite. The various sizes of the minerals lead a quite heterogeneous porous pattern inside the material.

The sample comes from a gallery of the ANDRA underground research laboratory at Bure (France). Its raw water content is 5.4% and its dry density is $2.24 g.cm^{-3}$. Mohajerani (2011) reviewed physical properties of the COX argillite available in bibliography. The dry density is typical to the France, eastern argillite (Heitz & Hitcher, 2002). The water content of the material is in the range of other studies (Wright 2001, Bauer-Plaindoux et al. 1998). M'Jahad (2013) cited various existing retention curves for this material. The water retention curve used here (Fig. 1) was acquired by Gerard (2011). The parameters of the van Genuchten model fitted on the water retention curve are presented in Tab. 1.

Table 1: Fitted van Genuchten parameters for COX argillite using the data by M'Jahad (2013).

α (MPa^{-1})	m	n
0.037	0.396	1.654

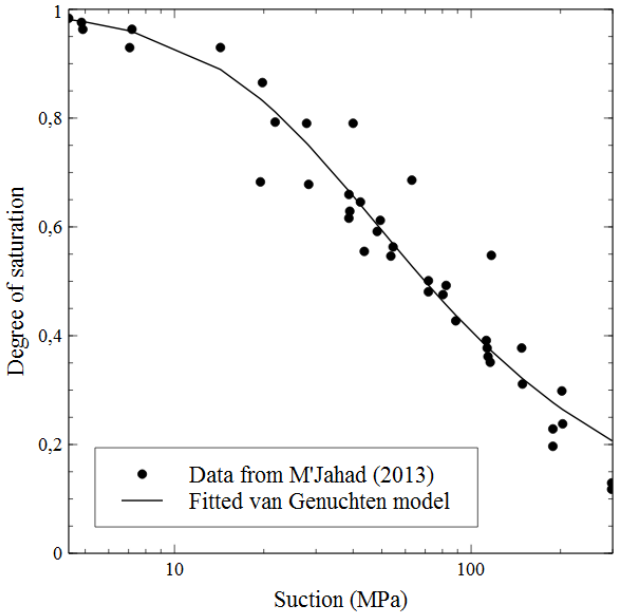

Figure 1. Water retention curve of COX argillite (Gerard 2011 cited by M'Jahad 2013).

2.4 *Sample preparation*

COX argillite was prepared in two ways in this study. First, crushed argillite was compacted at various water contents and densities. These samples allow performing the calibration curve to connect the MRI signal to water content of samples. Second, drying tests were applied on a sample of raw argillite.

The argillite was crushed then mixed with water in order to reach the desired mass water content ($9\% < w < 40\%$). The hydrated material was packed in hermetic bags and left to homogenize for at least 24 hours. 12 cylindrical samples of 30mm height were compacted in 2 layers in a mold 22mm in diameter. A sample had a dry density of $2 g.cm^{-3}$ whereas the 11 others samples had a dry density of $1.65 g.cm^{-3}$ (Table 1). The samples S1 to S11 were used to develop the T_2* vs. w calibration curve. After the MRI test, the final w_f, reported on Table 2, was verified by ignition loss (AFNOR 1995).

Table 2. Water contents at the end of the test (w_f) and dry densities (ρd) of the samples.

Samples	w_f (%)	ρd ($g.cm^{-3}$)	Samples	w_f (%)	ρd ($g.cm^{-3}$)
S1	9.9	1.65	S7	23.1	1.65
S2	11.6	1.65	S8	24.9	1.65
S3	14.1	1.65	S9	27.1	1.65
S4	16.4	1.65	S10	29.3	1.65
S5	18.5	1.65	S11	38.3	1.65
S6	19.6	1.65	S12	14.1	2.00

For the drying tests, a sample of 38mm in diameter and 76mm in height was cored in the raw argillite. The sample, enclosed in a Teflon mold, was submitted to two successive thermal solicitations. Before each solicitation, the sample was saturated. To ensure an efficient saturation, a porous rock was

placed at the top of the sample and the mold was merged upside down in distilled water for, at least, 50 days (Fig. 2a). The bottom of the mold was then closed and the top of the mold was open during the thermo-hydraulical solicitation (Fig. 2b). Finally, the mold was hermetically closed during the MRI test (Fig. 2c). The first solicitation consisted of putting the sample into a dessicator that includes a salt solution during 144 h (6 days). The salt solution was a magnesium chloride which imposed a relative humidity of 33% into the dessicator. For the second solicitation, the sample was placed in a climatic chamber with temperature regulated at 40°C and the relative hygrometry (RH) at 33%. The two solicitations are applied on the same sample with the same mineralogy and porous pattern.

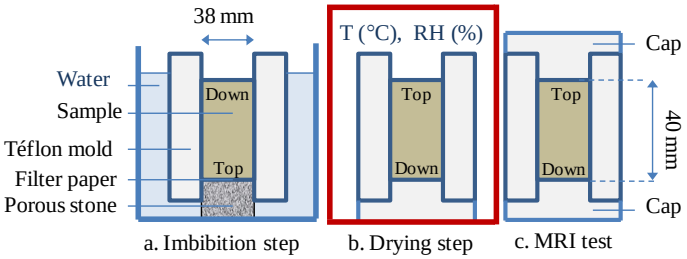

Figure 2. Successive steps of the study

3 RESULTS

In this part, the calibration curve obtained on compacted powders of argillite is first presented. Then the curve is used on drying tests performed on raw argillite samples. Finally, the unsaturated hydraulic conductivities of the samples are calculated.

3.1 *MRI calibration curve*

The calibration curve connects the T_2* deduced from MRI measurements and the water content of the sample. The T_2* obtained for the 12 samples of compacted argillite powder are reported in Figure 3.
A linear regression on samples S1 to S11 (Table 2) allows modeling the relationship between the T_2* values and the w for a dry density of 1.65g.cm^{-3}:

$$T_2^* = 1.1597w + 18.256 \quad (4)$$

The calibration curve (Fig. 3) is defined for water contents higher than 10%. However, the water content may be lower than 10% during the drying test. The calibration curve has to be complete for lowest water contents.

The result acquired on the sample compacted at a dry density of 2g.cm^{-3} is perfectly aligned with the other results obtained on sample at a dry density of 1.65g.cm^{-3}. According to this result, it seems that the density of the material has a negligible impact on the result. Also, this calibration curve may be used to characterize the raw material. This point will be verified in following studies.

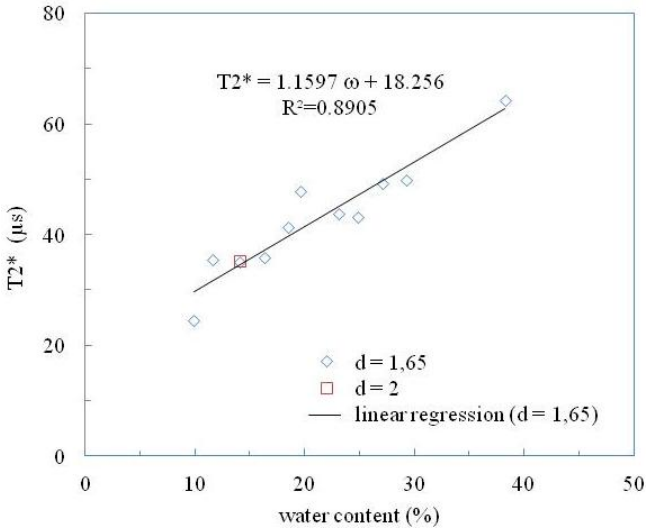

Figure 3. Calibration curve

3.2 *Drying tests*

During the first drying test, the material was submitted to air at 20°C and to a relative humidity of 33%. At various times step, the sample was extracted from the container, closed and then tested in the MRI. To allow the comparison between the two tests, the reduced water content, $\bar{w}$, is defined as follow :

$$\bar{w} = \frac{w}{w_i} \times 100 \quad (5)$$

Where w_i = initial water content (%).
Results are presented in Figure 4a. Only the first 35mm of the sample are analyzed by MRI. At the beginning of the test, the sample was well saturated and homogenous in depth with a $\bar{w}$ near to 100%. The values may be disturbed by the probable heterogeneity of the porous pattern inside the sample.
Over time, we observed the drying of the sample (Fig. 4). In the first 24h of test, the drying is more rapid on top of the sample (Depth=0) than on the bottom (Depth=35mm). $\bar{w}$ reaches 61% on the top whereas $\bar{w}$ on the bottom is not far from 100% (93%). During the next 40h, $\bar{w}$ evolves on the top as well as on the bottom of the sample. The evolution between 72h of drying and 144h of drying is very low. At the end of the test, the top $\bar{w}$ reaches 39.4% and the bottom $\bar{w}$ reaches 66%.
At the end of the first drying test, the sample was placed under imbibitions conditions in order to saturate the sample. A new drying test was next realized at 40°C and 33% RH. At the beginning of the test, $\bar{w}$ is not homogenous: on the top of the sample $\bar{w}$ is near to 100% whereas on the bottom, $\bar{w}$ is only 93%. During the first 2 h of test, a global homogenization is recorded and after 3h of test a drying is ob-

served on the top of the sample. In the following tests, homogenization time must be respected before the beginning of the drying. After 5 drying hours, the upper 10mm of the sample was affected. During the 15 following hours, this drying front makes progress to reach 20 mm. The three profiles obtained after 20h, 23h and 26h are superimposed. During the following hours, $\underline{w}$ decreases slowly at the top of the sample but highly at the bottom. $\underline{w}$ reaches an equilibrium value in relation with the temperature and the relative humidity imposed to the sample. At the end of the test, after 90 drying hours, the top $\underline{w}$ reaches 45% and the bottom $\underline{w}$ reaches 71%. These values are similar to the test at 20°C but the initial state was different.

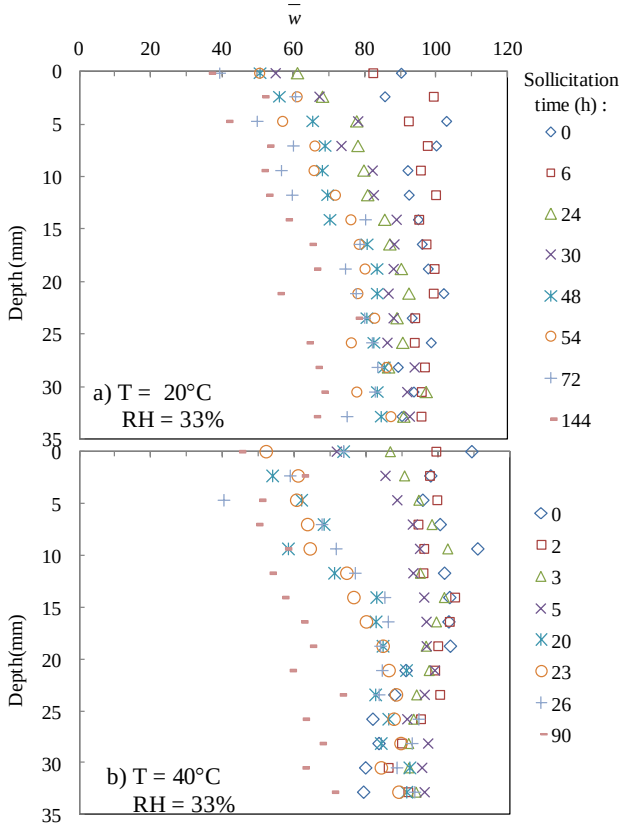

Figure 4. Drying tests on raw argillite submitted to a) T = 20°C and RH = 33%; b) T= 40°C and RH = 33%.

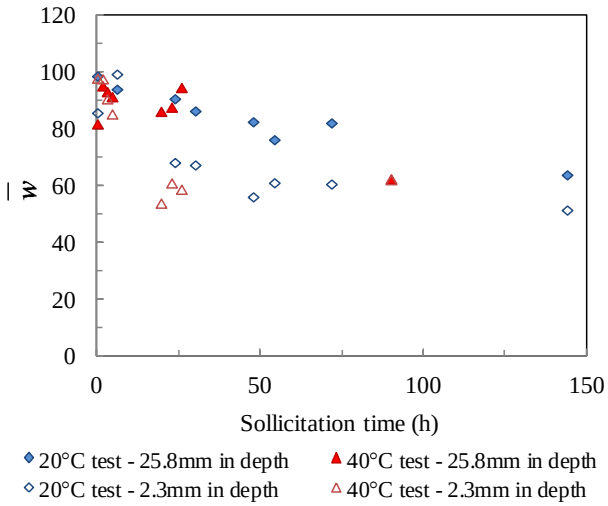

Figure 5. Reduced water content evolution along the time for the two drying tests at two depths (2.3mm and 25.8mm).

The Figure 5 provides for each test the evolution of $\underline{w}$ along the time on two points of the sample: at 2.3 mm and at 25.8 mm in depth. $\underline{w}$ decreases quickly during the first testing hours. As expected, the material at 25.8mm in depth is less affected by the drying than material at 2.3mm in depth. The evolution at 20°C is similar to the evolution at 40°C.

3.3 *Unsaturated hydraulic conductivities*

At each depth, the flow velocity and the hydraulic gradient are calculated from water content profiles and suction profiles respectively. Then the unsaturated hydraulic conductivity is determined using Darcy law (Equation 3). Results for the two tests are presented in figure 6.

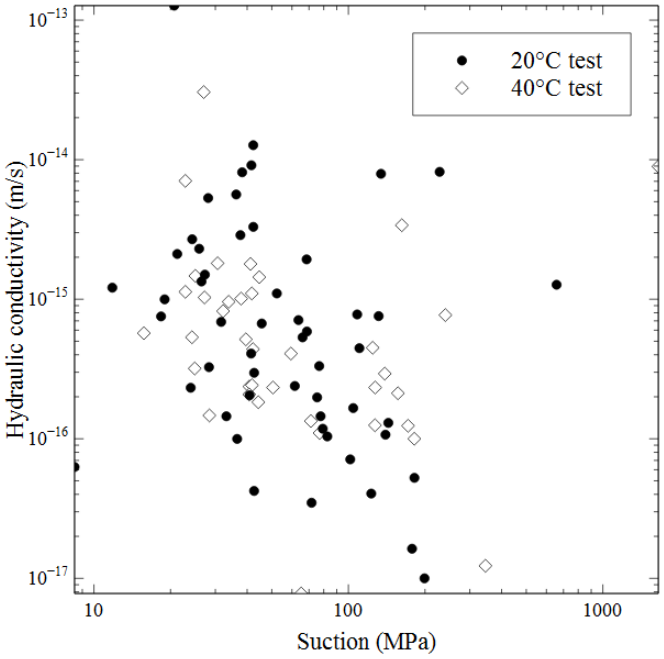

Figure 6. Unsaturated hydraulic conductivity curves derived from the tests.

The points are scattered in the figure due to the non monotonic evolution of the water content with the depth (Fig. 4). However, clear trends are highlighted. As expected, the unsaturated hydraulic conductivity decreases with the suction increasing. The results from tests realized at 20°C are superimposed to results from tests realized at 40°C in accordance with the measured values.

The unsaturated hydraulic conductivities calculated on the material are on a compatible order of magnitude than the hydraulic conductivity of 7. 10^{-13} m/s calculated by Enssle et al. (2001). These authors specify that the permeability values are in good agreement with those determined with hydraulic testing in boreholes.

4 CONCLUSION

In this study, a Single Point Imaging method is applied on clayey samples. A calibration curve which connects MRI signal to water content of samples was acquired on compacted samples. Two drying tests, at 20 and 40°C are performed on a raw argilite. The evolution of the water content inside the sample was observed over time. These results allow calculating the unsaturated hydraulic conductivity according to the instantaneous profile method. The unsaturated water conductivity are in good agreement with saturated conductivity measured in bibliography.

The method succeeds to detect a water content profile evolution without destroying the sample. As expected, the water content evolution is quicker on the top of the sample, which is in contact with air, than on the bottom. In this study, a temperature impact on the drying kinetic is not evidenced. However, the temperature range is very low and the uncertainty on the water content value remains quite important, especially at lowest water content values. Method development has to be carried on in order to improve the result.

5 AKNOWLEDGEMENT

This study was realized thanks to the ANDRA and GNR Forpro sponsoring.

6 REFERENCES

AFNOR 1995. *NF P94-050, Sols: reconnaissance et essais; Détermination de la teneur en eau pondérale des matériaux,* Association Française de Normalisation, Paris, France, 8p.

Abou-Chakra Guéry, A., Cormery, F.,. Shao J.F. & Kondo, D. 2008. A micromechanical model of elastoplastic and damage behavior of a cohesive geomaterial. *International Journal of Solids and Structures* 45: 1406–1429

Amin, M.H.G, Hall, L.D., Chorley, R.J., Richards, K.S., Carpenter, T.A. & Bache B.W. 1996. Visualization of static and dynamic water phenomenon in soil using magnetic resonance imaging, in: V.P. Singh, B. Kumar (Eds.), *Subsurface water Hydrology*, Kluwer Academic, Dordrecht, pp. 3–16.

Bauer-Plaindoux, C., Tessier, D., Ghoreychi M. 1998. *Propriétés mécaniques des roches argileuses carbonatées : importance de la relation calcite-argile.* C.R. Acad. Sci. IIa, 326.

Dvinskikh, S.V., Szutkowski, K. & Furó, I. 2009. MRI profiles over very wide concentration ranges: application to swelling of a bentonite clay. *Journal of magnetic resonance* 198: 146-150

Emid, S. & Creyghton, J.H.N. 1985. High resolution NMR imaging in solids. *Physica B* 128: 81-83$

Enssle, C.P., Cruchaudet, M, Croisé, J.& Brommundt, J. 2011. Determination of the permeability of the Callovo-Oxfordian clay at the metre to decametre scale, *Physics and Chemistry of the Earth* 36, 1669-1678.

Gerard, P. 2011. *Impact des transferts de gaz sur le comportement poro-mécanique des matériaux argileux*, PhD Thesis, Université de Liège.

Hamilton J., Daniel D.E. & Olson R.E. 1981. Measurement of hydraulic conductivity of partially saturated soils ; permeability and groundwater contaminant transport. *American Soc. for Testing and Material*, STP 746, Zimmie & Riggs Eds., 183-196.

Heitz J.F & Hicher P.Y. 2002 The mechanical behaviour of argillaceous rocks – Some questions from laboratory experiments. Proc. Int. *Symp. Hydromechanical and Thermohydromechanical Behaviour of Deep Argillaceous Rock*, 2002; pp 99–108.

Huang, Y. 2012.*Modélisation micromécanique du comportement différé des roches argileuses : application au stockage des déchets radioactifs.* PhD Thesis, Université de Lilles 1, 135p.

Koptyug, I.V. 2012. MRI of mass transport in porous media: Drying and sorption processes. *Progress in Nuclear Magnetic Resonance Spectroscopy* 65: 1–65.

Magat, J. 2008. *Apport de l'Imagerie par Résonance Magnétique dans l'étude des mécanismes de structuration des matériaux cimentaires : application au suivi des modifications engendrées par le séchage.* PhD thesis, Laboratoire Central des Ponts et Chaussées (LCPC), Paristech, ENPC, 190p.

Masrouri, F., Bicalho, K.V., Kawai, K. 2008. *Laborathry Hydraulic testing in unsaturated soils.* Geotech. Geol. Eng. 26 : 691-704.

M'Jahad, S. 2013. *Impact de la fissuration sur les propriétés de rétention d'eau et de transport de gaz des géométraux. Application au stockage profond des déchets radioactifs.* PhD thesis, Ecole Centrale de Lilles, France, 355p.

Mohajerani, M. 2011. Etude expérimentale du comportement thermo-hydro-mécanique de l'argilite du Callovo-Oxfordien. PhD thesis, Laboratoire Central des Ponts et Chaussées (LCPC), Paristech, ENPC, 274p.

Prebble, R.E.& Currie J.A. 1970. Soil water measurement by a low-resolution nuclear magnetic resonance technique. *Soil Sci.* 21: 273–288.

Simpson, A. J., McNally, D. J.& Simpson M. J. 2011. NMR spectroscopy in environmental research: From molecular interactions to global processes. *Progress in Nuclear Magnetic Resonance Spectroscopy* 58: 97–175.

Tsang, C.F., Barnichon, J.D., Birkholzer, J., Li, X.L., Liu, H.H. & Sillen X. 2011.Coupled thermo-hydro-mechanical processes in the near field of a high-level radioactive waste repository in clay formations. *International Journal of Rock Mechanics & Mining Sciences* 49: 31–44.

Van Genuchten, M.T. 1980. A closed-form equation for predicting the hydraulic conductivity of unsaturated soils. *Soil Science Society of America Journal*, 44, 1892-1898.

Wind, G.P. 1968. Capillary conductivity data estimated by a simple method. *Water in the unsaturated zone*, proc. of the Wageningen Symposium, ed. Rijtema & Wassink, vol. 1:181-191.

Write H. 2001. *Rôle de la minéralogie, de la texture et de la structure dans la déformation et la rupture des argilite de l'Est.* PhD thesis, Laboratoire Central des Ponts et Chaussées (LCPC), Paristech, ENPC.

Young, J.J., Bremner, T.W., Thomas, M.D.A., Balcom, B.J. 2006. Pure Phase Encode Magnetic Resonance Imaging of Concrete Building Materials. In Stapf, S.S. & Han, S.I. (eds), *NMR Imaging in chemical engineering*, Wiley-VCH, Germany, 285-303.